This manuscript is under revision in Geomorphology, and is not peer-reviewed.

Please feel free to contact any of the authors with feedback and suggestions for improvements.

Document history

Date	Action
08/Aug/2024	MS sent to co-authors for final draft acceptance
	Supplementary materials uploaded to Zenodo
12/Aug/2024	MS Submitted to EarthArXiv
15/Aug/2024	MS submitted to scientific journal for publication
5/Oct/2024	Received comments by reviewers
27/Dec/2024	Revised version submitted to Geomorphology

Reconstructing past sea-level changes from storm-built beach ridges

Preprint, compiled December 22, 2024

Alessio Rovere[1,2*], **Marta Pappalardo**[3], **Sebastian Richiano**[4], **Deirdre D. Ryan**[3], **Karla Rubio-Sandoval**[2], **Patricio Martin Ruiz**[5], **Alejandro Montes**[6,7], **and Evan J. Gowan**[8,9]

[1]DAIS, Department for environmental sciences, statistics and informatics, Ca' Foscari University of Venice, Venice, Italy
[2]MARUM, Center for Marine Environmental Sciences, University of Bremen, Bremen, Germany
[3]Department of Earth Sciences, University of Pisa, Pisa, Italy
[4]National Scientific and Technical Research Council, Instituto Patagónico de Geología y Paleontología, Puerto Madryn, Argentina
[5]Departamento de Geología, Universidad Nacional de la Patagonia San Juan Bosco, Comodoro Rivadavia, Chubut.
[6]CADIC-CONICET, Centro Austral de Investigaciones Científicas, Consejo Nacional de Investigaciones Científicas y Técnicas, Ushuaia, Argentina
[7]ICPA, Instituto de Ciencias Polares, Ambiente y Recursos Naturales, Universidad Nacional de Tierra del Fuego e Islas del Atlántico Sur, Ushuaia, Argentina
[8]Department of Earth and Environmental Sciences, Kumamoto University, Kumamoto, Japan
[9]KIKAI Institute for Coral Reef Sciences, Kagoshima, Japan

Abstract

Storm-built beach ridges, built by waves on sedimentary coasts, can be used as geomorphological indicators of past sea level. However, quantifying the relationship between the geomorphological elements of the ridge and the paleo sea level at the time of deposition is difficult, as a beach ridge is primarily correlated to wave energy and only secondarily to the position of sea level. In this work, we propose a methodology to quantify the upper and lower limits of a storm-built beach ridge based on remote sensing data. We use the tidal model FES2022, data from the Copernicus Marine Service and beach slope gathered from satellite imagery as inputs to different wave runup models, that are used to calculate the limits of the storm-built beach ridge. We test our approach on a particularly well-preserved Pleistocene storm-built beach ridge in Patagonia, Argentina. Our results show that the paleo relative sea level reconstructed using remote sensing data coincides (82.8% similarity) with that obtained from measured modern analog landforms at the same location.

***K*eywords** Pleistocene sea level · Beach ridges · Patagonia, Argentina · Paleo sea level

1 Introduction

Beach ridges are shore-parallel elongated mounds, occurring as single features or in sets, backing the coastline (Taylor and Stone, 1996; Hesp, 2006; Otvos, 2020) and formed by coastal processes. Different types of beach ridges have been described, categorized based on morphological and sedimentological features (Otvos, 2020). They are considered as originally being deposited by swash during high or low wave-energy conditions, but some models account for their genesis as the product of aggradation of an offshore bar. Regardless the typology, all beach ridges are considered as progradational features.

Storm-built beach ridges on sedimentary coasts are created by the accumulation of sediments by waves above sea level (Tamura, 2012). The observation of beach ridges (that Charles Lyell defined "shingle beaches" in his "Principles of Geology", Lyell, 1837), and their use as proxies for the past position of relative sea level (RSL, that is local sea level uncorrected for vertical land motions), dates back at least to Charles Darwin who, on his voyage through South America, described several beach ridges with embedded shells and discussed their relationship with past positions of the shoreline (Darwin, 1846).

While coastal landforms (such as beach ridges) can be described with classic geologic methods, quantifying their relationship with a former sea level requires rigorous approaches, that have been employed since the mid-80s (Van de Plassche 2013, first edited in 1986, and Shennan, 1986). Recently, the *"Handbook of sea-level research"* by Shennan (2015) has collected the main methods that are currently used to study former sea-level changes, which have been since then successfully used to build global sea-level databases for different time periods (Khan et al., 2019; Rovere et al., 2023). One key concept is that a geomorphological feature can be considered a sea-level index point if three key properties are known: i) its position and elevation measured with the highest possible accuracy; ii) its age of formation; iii) its relationship with sea level at the time of its formation. This relationship is called the *"indicative meaning"* (Shennan, 1986).

The indicative meaning is composed by two numerical values. The indicative range (IR) represents the vertical elevation range occupied by a sea-level index point, relative to contemporary tidal datums. The reference water level (RWL) is the distance between the midpoint of the IR and the former tidal datum, and represents the elevational difference between the sea-level index point and the former sea-level (expressed as a former tidal datum, such as Mean Sea Level). The best way to quantify the indicative meaning of a sea-level index point is to measure a modern analog and apply the elevation offset (and associated uncertainty) between the modern sea-level and the modern feature to the paleo context (Shennan, 2015).

*correspondence: alessio.rovere@unive.it

Several authors have used storm-built beach ridges as paleo sea-level index points. In particular, methods for extracting paleo sea-level information from the nearshore-shoreface inflection point on beach ridge systems surveyed with shallow surface geophysical techniques (e.g., ground-penetrating radar) have seen significant development (e.g. Brooke et al., 2019; Kumar et al., 2024). However, approaches for determining the indicative meaning of beach ridges in the absence of subsurface data remain underdeveloped.

Specifically, several studies have examined the surface elevation (or the elevation of sedimentary or biological elements near the surface) of Pleistocene beach ridges along the Atlantic coasts of Argentina and Uruguay (e.g. Rostami et al., 2000; Schellmann and Radtke, 2000; Zanchetta et al., 2012; Martínez and Rojas, 2013; Pappalardo et al., 2015; Rovere et al., 2020). However, in comparison with other regions, these features are rarely described in the literature, complicating efforts to compile sea-level data (Gowan et al., 2021).

In this study, we present a method to determine the indicative meaning of a storm-built beach ridge using remote sensing data. Building on recent research and established definitions (Lorscheid and Rovere, 2019; Rubio-Sandoval et al., 2024), the method integrates modern wave and tidal data with wave runup models and beach slope extraction from satellite imagery. We apply this approach to a benchmark site in central Patagonia, Argentina (south of the town of Caleta Olivia, Santa Cruz Province), where both the modern analog and the stratigraphy of the fossil beach ridge are well-defined and have been constrained through field surveys.

2 BENCHMARK SITE

The site we use to benchmark our methodology (46°33’29.0” S, 67°25’59.9” W, hereafter called *"benchmark site"*) is located within a quarry site locally named *"Cantera Delgado"*, ~15 km south of the town of Caleta Olivia, in the central part of the San Jorge Gulf, ~1500 km south of Buenos Aires (Figure 1). In general, this area is located on a passive margin and is embedded within the South America Plate. Caleta Olivia is located along the central-southern coast of the Gulf of San Jorge, an intracratonic, extensional basin formed since the Mid- Jurassic between the two North Patagonian and Deseado Massifs (Ramos and Ghiglione, 2008).

In this area, several authors reported Holocene and Pleistocene beach ridges, that reach elevations of 10-20 meters above modern sea level (e.g., Codignotto, 1983; Codignotto et al., 1992; Schellmann, 1998; Rostami et al., 2000; Aguirre, 2003; Schellmann and Radtke, 2003; Ribolini et al., 2014; Richiano et al., 2021). Although the amount of literature on this site and the surrounding area is remarkable, so far there is no agreement on the interpretation of the beach ridges extensively occurring in this area as paleo-sea-level indicators. In fact, there is no correlation between their height and age, and in many cases the same height corresponds to different ages (e.g. Pleistocene/Holocene).

2.1 Survey methods

We used differential Global Navigation Satellite systems (GNSS) to measure the position and elevation of the modern beach profile (Figure 2 B) and the fossil beach ridge (Figure 2 C). We employed a single-band EMLID RS+ GNSS composed of a base and a rover unit communicating via radio. The base station was located in full view of the sky and was left static collecting data for ~2h and 42 minutes. The data collected from the base station were processed using the Precise Point Positioning service of the Natural Resources of Canada (NRCAN-PPP). This allowed gathering a corrected base position, which was then used to correct each rover point using the scripts available in Rovere (2021).

Data were originally recorded in WGS84 coordinates, with height above the ITRF2008 ellipsoid. Orthometric heights (above mean sea level) were then calculated subtracting the GEOIDEAR16 geoid height from the measured ellipsoid height. It was estimated that the GEOIDEAR16 has an overall vertical accuracy of 0.1 m (Piñón et al., 2018). It is worth noting that Pappalardo et al. (2019) surmised that in some areas of Patagonia, referring GNSS data to the GEOIDEAR16 geoid might be affected by large discrepancies if compared with the

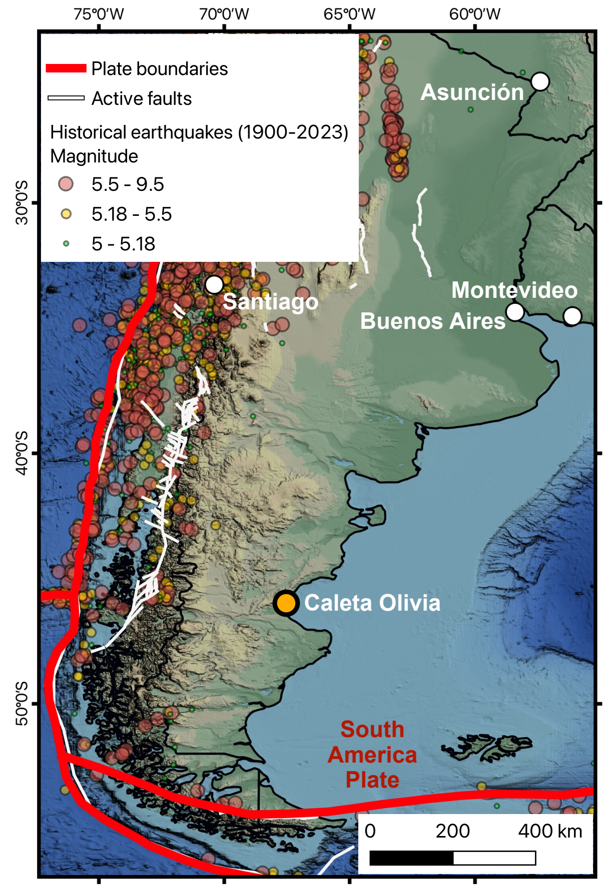

Figure 1: **Study area**. Location of the town of Caleta Olivia (the benchmark site is 15 km south of the town) within the Southern part of South America. Credits: Base map from Ryan et al. (2009). Active faults from Styron (2019) and plate boundaries derived from Bird (2003), as modified by Hugo Ahlenius and Nordpil on GitHub (`https://github.com/fraxen/tectonicplates`). Historical earthquakes from the US Geological Survey (2017).

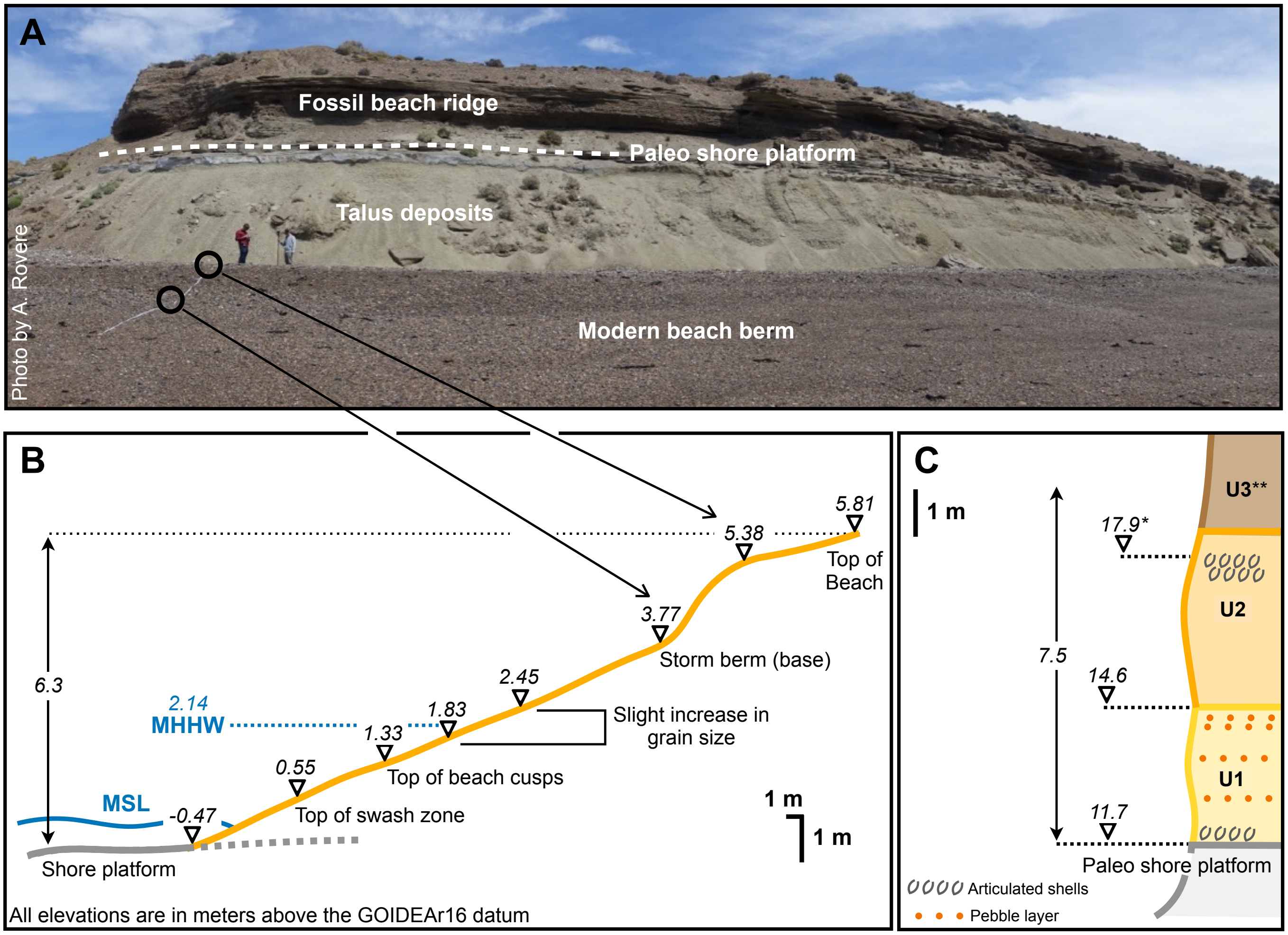

Figure 2: A) Composite photograph showing the modern beach berm (in the foreground) and the fossil beach ridge (in the background) at the benchmark site. B) GNSS profile of the modern beach with distinctive geomorphological elements. MSL = Mean Sea Level; MHHW = Mean Higher High Water. C) Stratigraphic section of the fossil (Pleistocene) beach ridge, divided into two units (U1 and U2). * indicates an elevation taken ~15 meters south of the section, as the point was not accessible on the vertical beach ridge face. ** Unit 3 was recognised at this section, but is more complete a few hundred meters from this section, and was described by Ribolini et al. (2014) starting at ~17m above sea level.

sea level datum obtained by tide gauge data. We remark that such discrepancy would not affect our results, as in the following sections we only compare elevation within this site, hence is it only relevant that the same elevation datum is used. However, we make available all the GNSS data collected in this work, that are originally referred to the ITRF2008 ellipsoid (see Supplementary Information for details).

The elevation error (σE) of each GNSS point surveyed in the field was calculated using the following formula:

$$\sigma E = \sqrt{GNSS_e^2 + Base_e^2 + Geoid_e^2} \qquad (1)$$

Where $GNSS_e$ is the error given as output by the GNSS system, $Base_e$ (only for data collected with the Base-Rover EMLID GNSS) is the elevation error of the base station, and $Geoid_e$ is the error associated with the GEOIDEAR16 (0.1 m). Overall, the 1σ elevation error associated to our measurements is 0.30 m.

2.2 *Modern beach*

The modern beach at our benchmark site (Figure 2 A,B) lies upon a shore platform, carved into the sedimentary rocks of the Monte León formation (which a few kilometers north, in the Chubut Province, is called Chenque formation) (Upper Oligocene / Lower Miocene, Martínez et al., 2020). Abrasion and subordinately bioerosion are apparently the main processes shaping this platform (Supplementary Figure 1) The shore platform can be observed at low tide (Supplementary Figure 1 B,C), and the contact with the beach deposits was measured at -0.47 m. The modern beach is characterized by beach cusps, at an elevation of 1.33 m. The grain size is between fine to very coarse gravels (4 to 64 mm diameter), with finer grain size close to the shore and a slight increase in grain size between the elevation of 1.83 and 2.45 m, which correspond to Mean Higher High Water (MHHW, 2.14 m). Above this level, a well-defined storm berm is a prominent geomorphological feature between 3.77 and 5.38 m. The modern storm berm appears laterally continuous, and at this location covers a ca. 1.5 m high cliff carved in an Holocene marine terrace which is clearly visible all along the coast N and S of the benchmark site (Ribolini et al., 2014). The beach deposits are covered by talus deposits created by quarried materials at 5.81 m.

2.3 *Pleistocene storm-built beach ridge*

The talus deposits covering the upper part of the modern beach have a resting angle of 30°- 40°(Figure 2 A), and are about 5m high. At ~10 m above sea level, the Monte Léon formation outcrops again. Here, it is cut by paleo marine abrasion, forming a fossil shore platform overlain by two sedimentary units with different characteristics. Unit 1 develops from 11.7 to 14.6 m in elevation (Figure 2 C, Supplementary Figure 2 A). At the base of this unit, very close to the contact with the shore platform, there are mollusk shells of the species *Ameghinomya antiqua* (formerly *Protothaca antiqua*) articulated but not in living position (Supplementary Figure 2 D). Unit 1 is composed by fine sands, interbedded by decimeter-wide layers characterized by coarser sediments (pebbles and gravels, Supplementary Figure 2 E). Towards the upper part of Unit 1, the coarser layers become more frequent up to the transition with Unit 2 (Supplementary Figure 2 C) and contain fragmented and disarticulated whole valves of *Ameghinomya antiqua*, as well as articulated valves. Unit 2 develops between 14.6 and ~18 m in elevation, and is characterized by an alternation of pebbles and gravels (Supplementary Figure 2 B) and by the presence, at its top, of a layer with articulated shells of *Ameghinomya antiqua*, not in living position.

A further unit (Unit 3), reaching up to 20.6 m, rests on top of Unit 2. This is a complex continental unit, described by Ribolini et al. (2014) a few hundred meters from the section reported in this paper, still within *"Cantera Delgado"*. Its bottom part is represented by silty sand with scattered pebbles displaying multiple pedogenetic carbonate crusts and incised by periglacial features (sand wedges). An aeolian sand cover seals the sequence. The formation of this continental unit was dated by Ribolini et al. (2014) to a time span encompassing the Last Glacial Maximum.

The location of our benchmark site coincides with that reported by Schellmann (1998) for samples Pa 124 to 126 (both *Ameghinomya antiqua* shells), that these authors collected between 16.5 and 18 meters above mean sea level (opossibly within Unit 2 described here). Six replicates of these samples were dated using Electron Spin Resonance, yielding ages ranging from 172±15 ka to 212±26 ka (hence consistent with Marine Isotopic Stage 7, Schellmann, 1998). Shells of the same species, were sampled by Schellmann (1998) at two other sites (Pa 70 and Pa 71), located 5.5 to 6.5 kilometers south of our benchmark site from horizons at ~10 and ~15 meters above sea level (Schellmann, 1998). These yielded ages consistent with Marine Isotopic Stage (MIS) 5e (~125 ka). In the same general area, at a site called *"Bahia Langara"* Rostami et al. (2000) obtained U-series ages consistent with MIS 5e at 16-17 m and with MIS 7 at 14 m above sea level (no vertical datum reported, assumed above mean sea level).

A definitive age attribution for this site lies beyond the scope of this study. Nonetheless, the data confirm that the surveyed beach ridge at the benchmark site is of Pleistocene age, likely corresponding to either MIS 5e or MIS 7. Similarly, evaluating the causes behind the ridge's elevated position relative to global mean sea level during these interglacials is outside the study's focus. However, we note that the observed elevation of the Pleistocene beach ridge in this region likely reflects the combined effects of global mean sea level, glacial isostatic adjustment, and mantle dynamic topography, which during previous interglacials can cause departures from eustasy of several meters Rubio-Sandoval et al., 2024.

3 Paleo RSL at the benchmark site

3.1 *Paleo RSL from modern analog*

The paleo storm beach ridge exposure at the benchmark site is a rare occurrence, at least within the Patagonian context (Blanco-Chao et al., 2014). In fact, quarrying works in *"Cantera Delgado"* produced a clear-cut section across its face, exposing the complete beach ridge sequence, from the paleo shore platform up to the highest deposits. At most other locations only parts of the beach ridge (usually the upper parts, showing articulated shells as those in U2, Figure 2) are exposed. The advantage of this peculiar exposure is that it is possible to better evaluate the indicative meaning of the beach ridge, and give a robust quantification of RSL at this site. This is one of the few places along the Atlantic coast of Patagonia where a shore platform outcrops beneath the beach (Blanco-Chao et al., 2014), providing the possibility to use it as a modern analog for paleo sea-level reconstructions.

The geomorphological element of Patagonian beach ridges that is often correlated to paleo sea level is a layer embedded within coarse gravels or pebbles composing the ridge, characterized by articulated shells of *Ameghinomya antiqua*. At the benchmark site, this layer is embedded within Unit 2 at 17.9 m above modern sea level (Figure 2 C). While in the study area at the time of survey we could not observe a modern analog shelly deposit on the ridge, in the regional context similar accumulations of articulated shells are observed between the ordinary berm (or the swash zone of ordinary waves) and the storm berm (Figure 3). In our modern beach profile, the top of the swash zone can be approximated by the top of beach cusps (1.33 m) and the top of the storm berm (5.38 m). Applying these two values of upper and lower limits of the indicative range, we estimate that paleo RSL at the time of formation of the beach ridge was **14.5 ± 2 m**, 1σ.

The occurrence in the benchmark site of both the modern and a paleo shore platform, the latter outcropping underneath the Pleistocene storm-built beach ridge, provides a further possibility to calculate paleo RSL. This can be done accepting a number of approximations. In macrotidal and high-energy environments, similar shore platforms are often considered as intertidal features (Sunamura, 1992).

We assume that the elevation at which the paleo shore platform was measured (11.7 m, Figure 2 C) was originally located be-

Figure 3: Accumulation of articulated and disarticulated mollusk shells (white among the gray gravel sands) on the modern beach at Mazarredo, ~80 km south of the benchmark site.

tween mean sea level and Mean Lower Low Water (MLLW), corresponding to the shore platform outer edge. This could be an overestimation if the seaward portion of the former shore platform had been extensively eroded by the Holocene RSL transgression. The presence of the Holocene terrace underneath the modern storm berm (reported in Ribolini et al., 2014), though, suggests that this was not the case. Consequently, the the upper and lower limits of the indicative range are assumed to be respectively Mean Sea Level (MSL) and MLLW. Their current position can be calculated assuming that the point measured at -0.47 broadly corresponds to the shore platform inner edge (Figure 2 B) and using 4.28 as the tidal range. Paleo RSL at the time of the shore platform formation was **15.4 ± 1.1 m**, 1σ.

3.2 Paleo RSL from runup models - previous approaches

While the most reliable methodology to calculate paleo RSL from a storm beach ridge is the use of a modern analog as described in the previous section, this kind of information is not always available. For this reason, various approaches have been proposed in the literature using proxies for wave runup. These are summarised in the sections below. The new approach proposed in this work is presented in section 4.

Most of the data reviewed within in the World Atlas of Last Interglacial shorelines (Rovere et al., 2023), including a recent review of Argentinian beach ridges (Gowan et al., 2021), make use of IMCalc (Lorscheid and Rovere, 2019) to calculate the indicative meaning of coastal landforms, among which beach ridges. This tool that allows to give a first-order quantification of the indicative meaning based on wave and tidal data in absence of data on modern analogs. For storm beach ridges, IMCalc uses the formula of Stockdon et al. (2006) to calculate the wave runup exceeded by 2% of the waves (R_2) at high tide (MHHW) in fair weather and storm wave conditions, and equating them to the elevation of, respectively, the ordinary and storm berm on an ideal beach profile, with a general slope (β) of 0.08. The significant wave height and period are extracted from wave data from the CAWCR (Collaboration for Australian Weather and Climate Research) wave hindcast (Durrant et al., 2013), which is based on the NOAA WaveWatch III wave model (Tolman et al., 2009) and the NCEP CFSR surface winds and sea ice data (Saha et al., 2010). For fair weather conditions, IMCalc uses average wave height and period, while for storm conditions, it uses the upper 2σ significant wave height and period. Using the IMCalc tool to calculate paleo RSL from the layer of articulated shells within Unit 2 (at 17.9 m), we obtain the a paleo RSL value of **15.9±0.7 m** (1σ).

Rubio-Sandoval et al. (2024) suggests a more detailed approach than IMCalc, that employs wave data measured by satellite altimetry and analysed with the RADWave software (Smith et al., 2020). This is a python package that provides access to altimeter datasets using the Australian Ocean Data Network (AODN) database, that contains data spanning from 1985 to present, validated and calibrated by Ribal and Young (2019). Wave data for the period Jan 2000 - Jan 2023 (Supplementary Figure 3) were then employed in a runup model ensamble implemented in the *py-wave-runup* tool (Leaman et al., 2020), also accounting for tides extracted from the FES2014 global tidal model (Lyard et al., 2021; Carrere et al., 2016). The beach slope was obtained with the CoastSat.Slope (Vos et al., 2020) tool. With this approach, we calculate that the upper limit of the indicative range for beach ridges at the benchmark site is 0.91 m, while the lower limit is 3.51 m (Supplementary Figure 3 B). Applying this range to the elevation of articulated shells of Unit 2 (17.9 m), we calculate that paleo RSL is **15.7±1.3 m** (1σ).

4 New approach to calculate the indicative meaning of beach ridges

Here, we build on the concept idealised in IMCalc and on the approach of Rubio-Sandoval et al. (2024) described above to build a workflow that allows calculating the indicative meaning for a beach ridge using the best datasets and tools available. We validate the results with the paleo RSL obtained at the benchmark site described above. The workflow is implemented in python and is divided in three steps, described below. Each step can be reproduced in other areas via the jupyter notebooks supporting this paper (Rovere, 2024a).

4.1 Tide and wave data

The first step of our methodology is to retrieve tidal and wave data from global datasets. Water level data over the period 01 Jan 1980 to 30 Sept 2023 (~43 years) was calculated using the FES2022 global tidal model (Carrere et al., 2022) at a point slightly offshore of the benchmark site (Figure 4 A). Using these data as input to the "CO-OPS Tidal Analysis DatumCalculator" (Licate et al., 2017) we calculate that MHHW is 2.14m and MLLW is - 2.14m (Figure 4 B).

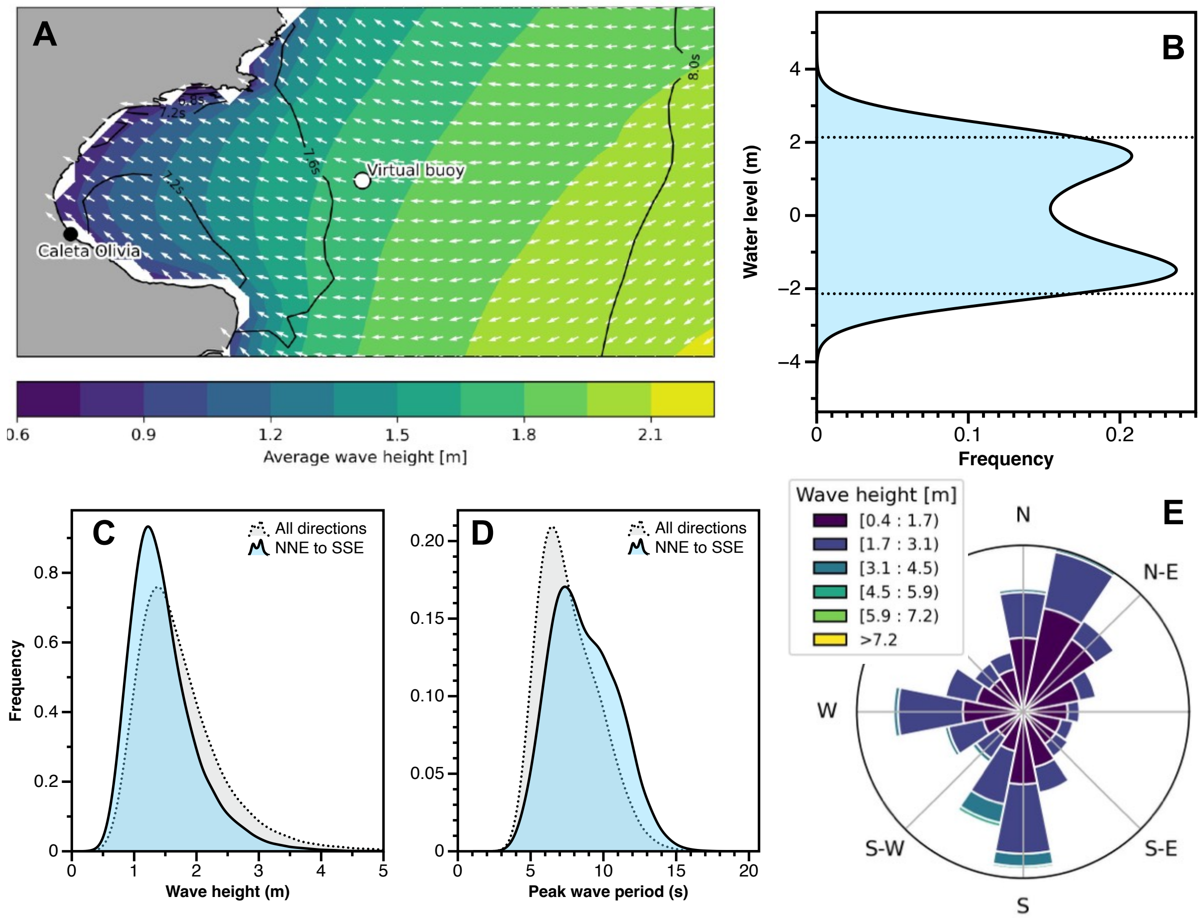

Figure 4: A) Average significant wave height (colored contours), wave perios (black lines) and direction(white arrows) in the study area extracted from the Copernicus Marine Environment Monitoring Service (CMEMS) WAVeReanalYSis (WAVERYS, Law-Chune et al., 2021), with indication of the point where wave data were extracted (virtual buoy). B) Smoothed histogram plot of tidal data extracted from the FES2022 model at Caleta Olivia (Carrere et al., 2022). The horizontal lines represent MHHW and MLLW calculated by the the "CO-OPS Tidal Analysis DatumCalculator" (Licate et al., 2017). C) and D) Smmoothed histogram plots of, respectively, significant wave height and period at the virtual buoy (location shown in panel A) for all directions (gray shade) and perpendicular to the coast (NNE to SSE, cyan shade). E) Wave rose for the virtual buoy (location shown in A).

Wave data is retrieved from the Copernicus Marine Environment Monitoring Service (CMEMS) WAVeReanalYSis (WAVERYS, Law-Chune et al., 2021). WAVERYS oceanic currents from the GLORYS12 physical ocean reanalysis (Lellouche et al., 2018) and assimilates wave heights from altimetry missions and directional wave spectra from Sentinel 1 synthetic aperture radar from 2017 onwards. This dataset spans the last ~43 years (01 Jan 1980 to 30 Sept 2023), sampled slightly offshore our benchmark site (Figure 4 A). In our area of interest, the waves directed towards the coast (with direction NNE to SSE) have a median significant wave height of 1.4 m and median significant wave period of 8 s (Figure 4 C,D), with main direction of waves from NNE ans South sectors (Figure 4 E).

4.2 Beach slope

Determining the beach slope (β) is a simple operation, that can be performed on any beach with basic topographic methods. At our benchmark site (Figure 2 B), it can be determined by dividing the difference between the base of the storm berm (3.77 m) and the top of swash zone (0.55 m) by the distance between the two (30.5 m). With this operation, we can determine that β is 0.1.

If no modern analog data is available, calculating β becomes more difficult. It is possible to do it via satellite-derived shorelines with CoastSat.Slope (Vos et al., 2020), a tool implemented within the CoastSat software (Vos et al., 2019). Thanks to this software, we could download 350 satellite images from Landsat 5,7,8,9 and Sentinel 2, spanning from January 1986 to October 2024. Over a coastal stretch of ~1 km around our study site, we identified 5 transects (Figure 5 A), where we evaluated the evolution of the shoreline over the period of available imagery. Using the tidal data calculated as described above, CoastSat.Slope (Vos et al., 2020) calculated the beach slope along each transect, including a median value and 5-95% confidence intervals. We then calculate the distribution of possible slopes with a function that selects randomly a transect and then samples a random value generated within the confidence interval with the median (Slope) acting as the peak likelihood using a triangular distribu-

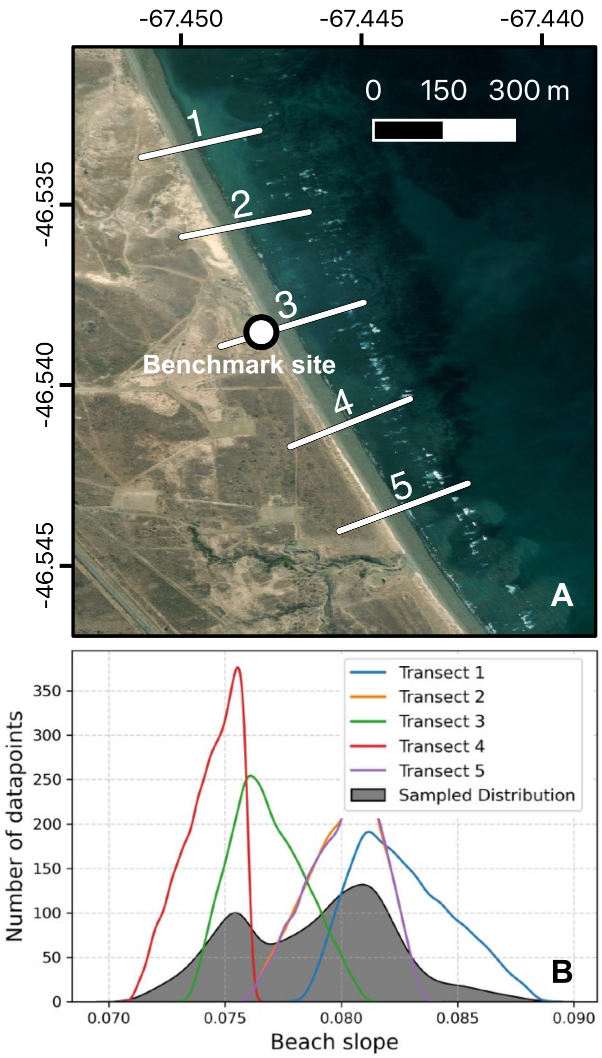

Figure 5: A) Satellite image of the study area, with transects 1-5 analysed in CoastSat to calculate the beach slope, and location of the benchmark site. Basemap sources: Esri, Maxar, Earthstar Geographics, and the GIS User Community. B) Slope calculated for each transect using satellite images and contemporaneous tidal levels (see Vos et al., 2020, for details on the methodology) and overall slope distribution calculated at the benchmark site.

tion (Figure 5 B). We calculate that the average β over the five transects is between 0.07 and 0.09 (grey distribution in Figure 5 B), which is in good agreement with what we measured in the field (0.1).

It is also worth noting that the results of this processing show that this beach, at the net of seasonal variations, has been rather stable throughout the last ~38 years (Supplementary Figure 4). This is an important point, as it strengthens the assumption that the modern beach and the modern beach slope are representative of a steady-state, hence they are more representative of long-term conditions of this beach.

4.3 *Wave runup*

In the last step of our workflow, we use wave, tidal data, and the beach slope calculated above to simulate R_2. There are several approaches and several empirical formulas that have been proposed to calculate R_2 on sandy beaches (see a recent review by Gomes da Silva et al., 2020). The most common among these were compiled in the *py-wave-runup* tool (Leaman et al., 2020). Using this tool, we run nine models that require as input significant wave height, period and beach slope (Holman, 1986; Ruggiero et al., 2001; Stockdon et al., 2006; Nielsen, 2009; Senechal et al., 2011; Vousdoukas et al., 2012; Atkinson et al., 2017; Passarella et al., 2018; Power et al., 2019). For Power et al. (2019), which requires an estimate of the Hydraulic roughness length, we use the relationship suggested by Leaman et al. (2020) of 2.5 × D_{50}, where D_{50} (grain size) is set to 8mm. We run these models using as wave conditions those directed between NNE and SSE in the study area (Figure 4). We also consider only the waves hitting the coast when the tide is equal or above mean sea level, as we assume that waves hitting below MSL would produce ephemeral landforms, that are usually re-eroded within one or two tidal cycles.

We test the results of these models against the height of the swash zone measured at the time of our survey (0.55 m, Supplementary Figure 6). The modelled runup (corrected by the tide at the time of survey) shows good agreement with the observed reach of waves during the survey. Also the other morphological elements we observed on the modern beach fall within the probability density distribution of the modelled runup (Figure 6 A).

The modern runup is representative of the wave and tidal conditions over the period 1980-2024. Over an interglacial, it is possibile that the same storm measured in the modern happened at different stages of the tide. To account for this possibility, we create a synthetic dataset composed of one million different conditions of waves, tides and beach slope. The synthetic dataset is created by randomly sampling a pair of values for wave height and period, one tidal level above MSL and one value of beach slope (β) from the distribution shown in Figure 5 B. We then use this dataset as input to the runup models described above, obtaining the probability distribution shown in Figure 6 B.

We use this distribution to derive the indicative meaning of the storm beach ridge in the area, assuming that it would form between the 1st and 99th percentiles of the calculated wave runup. Under this assumption, the upper and lower limits of the indicative range would be, respectively, 4.5 m and 0.9 m (Figure 6 B). Using these values, we calculate that paleo RSL as indicated by the articulated shells layer at 17.9 m (Figure 2 C) is **15.2 ± 1.8 m** (1σ).

5 Discussion

From the measurement of the modern analog, we reconstruct that paleo RSL at the benchmark site used in this work is 14.5 ± 2 m. This is consistent with the interpretation of Unit 1, located below the articulated shells we used as index point, that was interpreted as forming in the lower intertidal / subtidal zone (Schellmann, 1998). The paleo RSL calculated from the beach ridge at this site is also confirmed by that derived

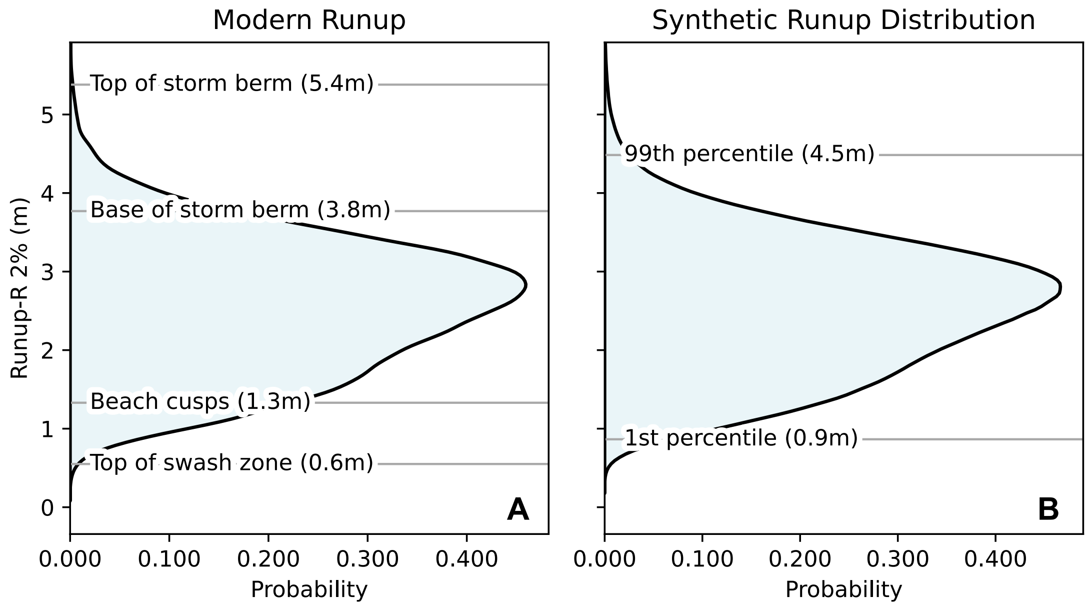

Figure 6: A) Probability density plots representing simulated 2% wave runup (R_2) at the benchmark site between 1980 and 2024, for waves with directions between NNE and SSE and reaching the coast in tidal conditions from MSL to high tide. Elements measured on the modern shoreline are plotted as grey lines with labels. A breakup of this histogram into the contribution of different runup models is shown in Supplementary Figure 5. B) Probability density plot representing simulated 2% wave runup at the benchmark site for the synthetic dataset, calculated as described in the main text. The grey lones show the 1^{st}st and 99^{th} percentiles of this distribution.

from the paleo shore platform, which sets paleo RSL at 15.4 ± 1.1 m (Figure 7). There is a striking similarity between the paleo RSL reconstructed from the modern analog and that derived from the runup-based reconstructions of Lorscheid and Rovere (2019), Rubio-Sandoval et al. (2024) and the one used in this work (Figure 7).

To quantify the similarity between the paleo RSL distributions obtained with runup models and the one gathered from the modern analog, we use the Kolmogorov-Smirnov test. The test returns a statistic D which is the maximum difference between the empirical distribution functions of the two samples. D varies between 0 and 1, with a lower D value indicating more similarity. We calculate the similarity in percentage as $(1-D)\times 100$. We calculate that the similarity between the paleo RSL calculated from the modern analog and that obtained from IMCalc is 49.7%. The same comparison with the method of Rubio-Sandoval et al. (2024) yields a similarity score of 67.8% and with the one from the workflow presented in this study, the similarity score improves to 82.8%. Compared to previous runup-based approaches, both IMCalc (Lorscheid and Rovere, 2019) and Rubio-Sandoval et al. (2024) reconstruct correctly the paleo RSL at the benchmark site, but they underestimate error bars.

While the methodology we proposed in this work performs well at the benchmark site, there are some caveats and limitations that must be considered when applying this work to other sites, with different characteristics. We discuss them hereafter.

The runup models employed in this study were mostly developed for sandy beaches, with relatively uniform nearshore slope. The benchmark site deviates from this pattern, as it is

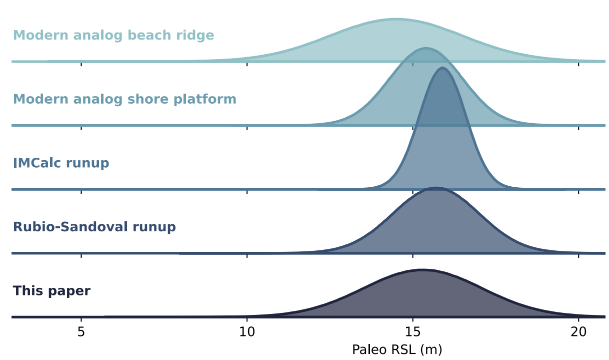

Figure 7: Comparison between paleo RSL calculated using indicative meaning estimated by the modern analog, IMCalc (Lorscheid and Rovere, 2019) and the methodology outlined in this work.

a gravel beach underlain by a shore platform. Despite this departure from the ideal case, our modelling chain performs well when runup values are compared to sedimentary structures on the beach (Figure 6 A) or with observed wave runup at the time of survey (Supplementary Figure 6). The little influence of the shore platform might be due to the fact that it outcrops only at low tide, allowing therefore waves to reach the shore and dissipate on the beach at high tide. The coarser grain size does not seem to affect much the runup values. In facr, the only runup model that takes into account grain size in the form of hydraulic roughness (Power et al., 2019) gives in fact results that do not deviate significantly from the other models (Supplementary Figure 5). As Power et al. (2019) highlight, *"wave height, wavelength, and beach slope are shown to be the three primary factors influencing wave runup, with grain size/bed roughness having a smaller, but still significant influence on the runup"*.

We have not tested the method we propose here on beaches that have been affected by significant erosion or that have been subject to significant vertical movement; either process may significantly altered beach slope over time. To account for this potential complication, we include in our workflow the analysis of shoreline variations through time (Supplementary Figure 4), where possible. This analysis may reveal any significant changes to the modern beach slope that would result in an inaccurate paleo runup model.

Another important caveat is related to the hydrodynamic boundary conditions we use in our workflow. Using modern tide and wave data, the implicit key assumption is that the wave intensity and tidal range were, in the area of interest, the same at the time of formation of the beach ridge as they are today. This might not be accurate.

Models of paleo tidal ranges during the Pleistocene are constrained to either discrete periods of time (Wilmes et al., 2023) or restricted geographic areas (Lorscheid et al., 2017). Substantially more work on tidal range changes and on their implication on the reconstruction of paleo RSL has been done for the Holocene (Horton et al., 2013; Sulzbach et al., 2023; Hill et al., 2011). A global model of tidal range changes for the Pleistocene interglacials does not exist, but it would allow correcting the runup calculations for different tides.

Also the intensity of waves in previous interglacials (more specifically in the Last Interglacial) has been widely debated, mostly on the basis of particular landforms (Rovere et al., 2017a; Hearty and Tormey, 2018; Rovere et al., 2018b). Models on the intensity and direction of storms and tropical cyclones suggest that it cannot be assumed that wave characteristics were the same between the present and the Last Interglacial (Kaspar et al., 2007; Yan et al., 2021; Huan et al., 2023), but models that quantify the change in significant wave height and period at the local scale that would be needed to correct our data are still missing.

Scussolini et al. (2023) provide global models of storm surges for extreme storms in the Last Interglacial which, for the area of interest, indicate that extreme storm surge would have been higher by 6 cm with respect to present-day (Supplementary Figure 7). This would not change substantially the paleo RSL calculated above. We note that, towards the Northern part of the San Jorge gulf, this assumption might not be true, and the upper limit of storm-built beach ridges would have to be corrected upwards by up to ~20 cm (Supplementary Figure 7).

6 CONCLUSIONS

Storm-built beach ridges are widely used, in particular along the Atlantic coasts, to reconstruct Holocene and Pleistocene sea-level changes. However, the modern analog of these landforms is less studied and is seldom reported in the literature. Our results show that it is possible to exploit freely available satellite-derived data and models that are commonly employed to study modern coastal processes to obtain a reliable estimate of the paleo RSL associated with beach ridges.

With our workflow, that is entirely based on remotely sensed data, we calculate paleo RSL at the benchmark site with similarity of 82.8% with respect to the paleo RSL calculated from modern analog data, outperforming previous similar approaches. We surmise that the approach proposed in this work may be used to better quantify the indicative meaning of fossil storm beach ridges.

It is also worth noting that, from the wave, tidal and runup data calculated by the workflow presented here, it may be possible to calculate the indicative meaning of other depositional sea-level index points, such as other types of beach deposit. As an example, the general definition of beach deposits entails that they form between the ordinary berm and the depth of closure of ordinary waves (Rovere et al., 2016), which can be easily quantified from wave data and runup models (Lorscheid and Rovere, 2019), such as those used in our workflow for beach ridges.

ACKNOWLEDGMENTS

Tidal data used in this work were extracted from FES2022, a product by NOVELTIS, LEGOS, CLS Space Oceanography Division and CNES. It is distributed by AVISO, with support from CNES (http://www.aviso.altimetry.fr/). Wave data was generated using the E.U. Copernicus Marine Service Information (https://data.marine.copernicus.eu/product/GLOBAL_MULTIYEAR_WAV_001_032/description). The basemap in Figure 5 was created using using ArcGIS® software by Esri. ArcGIS® and ArcMap™ are the intellectual property of Esri and are used herein under license. © Esri. All rights reserved. For more information about Esri®software, please visit www.esri.com. The authors acknowledge PALSEA for useful discussions during annual meetings. PALSEA is a working group of the International Union for Quaternary Sciences (INQUA) and Past Global Changes (PAGES), which in turn received support from the Swiss Academy of Sciences and the Chinese Academy of Sciences.

FUNDING

This project has received funding from the European Research Council (ERC) under the European Union's Horizon 2020 research and innovation programme (grant agreement no. 802414 to AR). EJG was funded by an International Postdoctoral Fellowship of Japan Society for the Promotion of Science, Helmholtz Exzellenznetzwerks "The Polar System and its Effects on the Ocean Floor (POSY)" and the Helmholtz Climate Initiative REKLIM (Regional Climate Change), a joint research project at the Helmholtz Association of German Research Centres (HGF), and also supported by the PACES II program at the Alfred Wegener Institute and the Bundesministerium für Bildung und Forschung-funded project, PalMod. SR acknowledges a fellowship by INQUA, and projects PUE-IPGP-CONICET and PICT2020A-1763.

Authors contributions

AR had the initial idea and wrote the paper with substantial input from MP. AR made the code for the workflow described in the paper. SR, AM and PMR provided insights on local geology, geomorphology and paleobiology. AR, MP, SR, DDR, KRS, PMR and EJG participated to different field campaigns at Caleta Olivia, that resulted in the data used for this paper. All authors revised the text, giving input according to their expertise, and agree with its contents.

Supplementary Information

The Supplementary Information to this paper contains all the raw data described in this paper and the jupyter notebooks to reproduce the results of this work and apply the same workflow in other areas. The pre-review version of the scripts is available as Rovere (2024b) and the final version is available as Rovere (2024a).

References

Aguirre, M. L. (2003). Late Pleistocene and Holocene palaeoenvironments in Golfo San Jorge, Patagonia: molluscan evidence. *Marine Geology 194*(1-2), 3–30.

Atkinson, A. L., H. E. Power, T. Moura, T. Hammond, D. P. Callaghan, and T. E. Baldock (2017). Assessment of runup predictions by empirical models on non-truncated beaches on the south-east Australian coast. *Coastal Engineering 119*, 15–31.

Bird, P. (2003). An updated digital model of plate boundaries. *Geochemistry, Geophysics, Geosystems 4*(3).

Blanco-Chao, R., K. Pedoja, C. Witt, J. Martinod, L. Husson, V. Regard, L. Audin, M. Nexer, B. Delcaillau, M. Saillard, D. Melnick, J. F. Dumont, E. Santana, E. Navarrete, C. Martillo, M. Pappalardo, L. Ayala, J. F. Araya, A. Feal-Pérez, D. Correa, and I. Arozarena-Llopis (2014). Chapter 10 The rock coast of South and Central America. *Geological Society, London, Memoirs 40*(1), 155–191.

Brooke, B. P., Z. Huang, W. A. Nicholas, T. S. Oliver, T. Tamura, C. D. Woodroffe, and S. L. Nichol (2019). Relative sea-level records preserved in holocene beach-ridge strandplains – an example from tropical northeastern australia. *Marine Geology 411*, 107–118.

Carrere, L., F. Lyard, M. Cancet, D. Allain, M.-L. Dabat, E. Fouchet, E. Sahuc, Y. Faugere, G. Dibarboure, and N. Picot (2022). A new barotropic tide model for global ocean: Fes2022. In *2022 Ocean Surface Topography Science Team Meeting*, pp. 43.

Carrere, L., F. Lyard, M. Cancet, A. Guillot, and N. Picot (2016). FES2014, a new tidal model–Validation results and perspectives for improvements, presentation to ESA Living Planet Conference.

Codignotto, J. (1983). Depósitos elevados y/o de acreción Pleistoceno-Holoceno en la costa Fueguino-Patagónica. In *Simposio Oscilaciones del nivel del mar durante el último hemiciclo deglacial en la Argentina*, pp. 12–26.

Codignotto, J. O., R. R. Kokot, and S. C. Marcomini (1992). Neotectonism and sea-level changes in the coastal zone of Argentina. *Journal of coastal research*, 125–133.

Darwin, C. (1846). *Geology of the Voyage of the Beagle, Under the Command of Capt. Fitzroy, RN During the Years 1832 to 1836: III*. Smith, Elder.

Durrant, T., M. Hemer, C. Trenham, and D. Greenslade (2013). CAWCR Wave Hindcast 1979–2010 v7. *CSIRO Data Collect*.

Gomes da Silva, P., G. Coco, R. Garnier, and A. H. Klein (2020). On the prediction of runup, setup and swash on beaches. *Earth-Science Reviews 204*, 103148.

Gowan, E. J., A. Rovere, D. D. Ryan, S. Richiano, A. Montes, M. Pappalardo, and M. L. Aguirre (2021). Last interglacial (MIS 5e) sea-level proxies in southeastern South America. *Earth System Science Data 13*(1), 171–197.

Hearty, P. J. and B. R. Tormey (2018). Listen to the whisper of the rocks, telling their ancient story. *Proceedings of the National Academy of Sciences 115*(13), E2902–E2903.

Hesp, P. (2006). Sand beach ridges: definitions and redefinition. *Journal of Coastal Research*, 72–75.

Hill, D. F., S. D. Griffiths, W. R. Peltier, B. P. Horton, and T. E. Törnqvist (2011). High-resolution numerical modeling of tides in the western Atlantic, Gulf of Mexico, and Caribbean Sea during the Holocene. *Journal of Geophysical Research: Oceans 116*(C10).

Holman, R. (1986). Extreme value statistics for wave run-up on a natural beach. *Coastal Engineering 9*(6), 527–544.

Horton, B. P., S. E. Engelhart, D. F. Hill, A. C. Kemp, D. Nikitina, K. G. Miller, and W. R. Peltier (2013). Influence of tidal-range change and sediment compaction on Holocene relative sea-level change in New Jersey, USA. *Journal of Quaternary Science 28*(4), 403–411.

Huan, D., Q. Yan, and T. Wei (2023). Unfavorable environmental conditions for tropical cyclone genesis over the western North Pacific during the Last Interglacial based on PMIP4 simulations. *Atmospheric and Oceanic Science Letters 16*(5), 100395.

Kaspar, F., T. Spangehl, and U. Cubasch (2007). Northern hemisphere winter storm tracks of the Eemian interglacial and the last glacial inception. *Climate of the Past 3*(2), 181–192.

Khan, N. S., B. P. Horton, S. Engelhart, A. Rovere, M. Vacchi, E. L. Ashe, T. E. Törnqvist, A. Dutton, M. P. Hijma, and I. Shennan (2019). Inception of a global atlas of sea levels since the Last Glacial Maximum. *Quaternary Science Reviews 220*, 359–371.

Kumar, R., A. D. Switzer, C. Gouramanis, C. S. Bristow, T. A. Shaw, K. Jankaew, T. Li, and D. Brill (2024). Late-holocene sea-level markers preserved in a beach ridge system on phra thong island, thailand. *Geomorphology 465*, 109405.

Law-Chune, S., L. Aouf, A. Dalphinet, B. Levier, Y. Drillet, and M. Drevillon (2021). WAVERYS: a CMEMS global wave reanalysis during the altimetry period. *Ocean Dynamics 71*, 357–378.

Leaman, C., T. Beuzen, and E. B. Goldstein (2020). chrisleaman/py-wave-runup: v0.1.10.

Lellouche, J.-M., E. Greiner, O. Le Galloudec, G. Garric, C. Regnier, M. Drevillon, M. Benkiran, C.-E. Testut, R. Bourdalle-Badie, F. Gasparin, et al. (2018). Recent updates to the Copernicus Marine Service global ocean monitoring and forecasting real-time 1/12 deg high-resolution system. *Ocean Science 14*(5), 1093–1126.

Licate, L. A., G. Dusek, and L. Huang (2017). A comparison of datums derived from CO-OPS verified data products and Tidal Analysis Datum Calculator.

Lorscheid, T., T. Felis, P. Stocchi, J. C. Obert, D. Scholz, and A. Rovere (2017). Tides in the Last Interglacial: insights from notch geometry and palaeo tidal models in Bonaire, Netherland Antilles. *Scientific Reports 7*(1), 16241.

Lorscheid, T. and A. Rovere (2019). The indicative meaning calculator–quantification of paleo sea-level relationships by using global wave and tide datasets. *Open Geospatial Data, Software and Standards 4*, 1–8.

Lyard, F. H., D. J. Allain, M. Cancet, L. Carrère, and N. Picot (2021). FES2014 global ocean tide atlas: design and performance. *Ocean Science 17*(3), 615–649.

Lyell, C. (1837). *Principles of geology: being an inquiry how far the former changes of the earth's surface are referable to causes now in operation*, Volume 1. J. Kay, jun. & brother.

Martínez, H., D. Molín, C. Nelson, S. E. Castro Godoy, F. Quintón Piegas Luna, H. G. Marengo, M. A. Dzendoletas, H. D. Pezzuchi, C. Parisi, J. L. A. Panza, et al. (2020). Hoja Geológica 4769-II Colonia Las Heras y Hoja Geológica 4766-I Bahía Lángara, Provincia de Santa Cruz.

Martínez, S. and A. Rojas (2013). Relative sea level during the Holocene in Uruguay. *Palaeogeography, Palaeoclimatology, Palaeoecology 374*, 123–131.

Nielsen, P. (2009). *Coastal and estuarine processes*, Volume 29. World Scientific Publishing Company.

Otvos, E. G. (2020). Coastal barriers - fresh look at origins, nomenclature and classification issues. *Geomorphology 355*, 107000.

Pappalardo, M., M. L. Aguirre, M. Bini, I. Consoloni, E. E. Fucks, J. Hellstrom, I. Isola, A. Ribolini, and G. Zanchetta (2015). Coastal landscape evolution and sea-level change: a case study from Central Patagonia (Argentina).

Pappalardo, M., C. Baroni, M. Bini, I. Isola, A. Ribolini, M. C. Salvatore, and G. Zanchetta (2019). Challenges in relative sea-level change assessment highlighted through a case study: The central coast of Atlantic Patagonia. *Global and Planetary Change 182*, 103008.

Passarella, M., E. B. Goldstein, S. De Muro, and G. Coco (2018). The use of genetic programming to develop a predictor of swash excursion on sandy beaches. *Natural Hazards and Earth System Sciences 18*(2), 599–611.

Piñón, D., K. Zhang, S. Wu, and S. Cimbaro (2018). A new argentinean gravimetric geoid model: GEOIDEAR. In *International Symposium on Earth and Environmental Sciences for Future Generations: Proceedings of the IAG General Assembly, Prague, Czech Republic, June 22-July 2, 2015*, pp. 53–62. Springer.

Power, H. E., B. Gharabaghi, H. Bonakdari, B. Robertson, A. L. Atkinson, and T. E. Baldock (2019). Prediction of wave runup on beaches using gene-expression programming and empirical relationships. *Coastal Engineering 144*, 47–61.

Ramos, V. A. and M. C. Ghiglione (2008). Tectonic evolution of the Patagonian Andes. *Developments in quaternary sciences 11*, 57–71.

Ribal, A. and I. R. Young (2019). 33 years of globally calibrated wave height and wind speed data based on altimeter observations. *Scientific data 6*(1), 77.

Ribolini, A., M. Bini, I. Consoloni, I. Isola, M. Pappalardo, G. Zanchetta, E. Fucks, L. Panzeri, M. Martini, and F. Terrasi (2014). Late-pleistocene wedge structures along the patagonian coast (argentina): chronological constraints and palaeoenvironmental implications. *Geografiska Annaler: Series A, Physical Geography 96*(2), 161–176.

Richiano, S., M. L. Aguirre, and L. Giachetti (2021). Bioerosion on marine Quaternary gastropods from the southern Golfo San Jorge, Patagonia, Argentina: What do they tell us? *Journal of South American Earth Sciences 107*, 103106.

Rostami, K., W. Peltier, and A. Mangini (2000). Quaternary marine terraces, sea-level changes and uplift history of Patagonia, Argentina: comparisons with predictions of the ICE-4G (VM2) model of the global process of glacial isostatic adjustment. *Quaternary Science Reviews 19*(14-15), 1495–1525.

Rovere, A. (2021). GPS-Utilities ver. 1.0.

Rovere, A. (2024a). Beach ridges runup models for paleo sea level applications.

Rovere, A. (2024b). Beach-ridges-runup: Pre-review version.

Rovere, A., E. Casella, D. L. Harris, T. Lorscheid, N. A. K. Nandasena, B. Dyer, M. R. Sandstrom, P. Stocchi, W. J. D'Andrea, and M. E. Raymo (2017a). Giant boulders and Last Interglacial storm intensity in the North Atlantic. *Proceedings of the National Academy of Sciences 114*(46), 201712433. Publisher: National Academy of Sciences.

Rovere, A., E. Casella, D. L. Harris, T. Lorscheid, N. A. K. Nandasena, B. Dyer, M. R. Sandstrom, P. Stocchi, W. J. D'Andrea, and M. E. Raymo (2018b). Reply to Hearty and Tormey: Use the scientific method to test geologic hypotheses, because rocks do not whisper. *Proceedings of the National Academy of Sciences*, 201800534.

Rovere, A., M. Pappalardo, S. Richiano, M. Aguirre, M. R. Sandstrom, P. J. Hearty, J. Austermann, I. Castellanos, and M. E. Raymo (2020). Higher than present global mean sea level recorded by an Early Pliocene intertidal unit in Patagonia (Argentina). *Communications Earth & Environment 1*(1), 68.

Rovere, A., M. E. Raymo, M. Vacchi, T. Lorscheid, P. Stocchi, L. Gómez-Pujol, D. L. Harris, E. Casella, M. J. O'Leary, and P. J. Hearty (2016). The analysis of Last Interglacial (MIS 5e) relative sea-level indicators: Reconstructing sea-level in a warmer world. *Earth-Science Reviews 159*, 404–427.

Rovere, A., D. D. Ryan, M. Vacchi, A. Dutton, A. R. Simms, and C. V. Murray-Wallace (2023). The World Atlas of Last Interglacial Shorelines (version 1.0). *Earth System Science Data 15*(1), 1–23.

Rubio-Sandoval, K., D. D. Ryan, S. Richiano, L. M. Giachetti, A. Hollyday, J. Bright, E. J. Gowan, M. Pappalardo, J. Austermann, D. S. Kaufman, and A. Rovere (2024). Quaternary and pliocene sea-level changes at camarones, central patagonia, argentina. *Quaternary Science Reviews 345*, 108999.

Ruggiero, P., P. D. Komar, W. G. McDougal, J. J. Marra, and R. A. Beach (2001). Wave runup, extreme water levels and the erosion of properties backing beaches. *Journal of coastal research*, 407–419.

Ryan, W. B. F., S. M. Carbotte, J. O. Coplan, S. O'Hara, A. Melkonian, R. Arko, R. A. Weissel, V. Ferrini, A. Goodwillie, F. Nitsche, J. Bonczkowski, and R. Zemsky (2009). Global Multi-Resolution Topography synthesis. *Geochemistry, Geophysics, Geosystems 10*(3).

Saha, S., S. Moorthi, H.-L. Pan, X. Wu, J. Wang, S. Nadiga, P. Tripp, R. Kistler, J. Woollen, D. Behringer, et al. (2010). The NCEP climate forecast system reanalysis. *Bulletin of the American Meteorological Society 91*(8), 1015–1058.

Schellmann, G. (1998). *Jungkänozoische Landschaftsgeschichte Patagoniens (Argentinien): andine Vorlandvergletscherungen, Talentwicklung und marine Terrassen*. 1. Auflage, Essen: Klartext, 1998.

Schellmann, G. and U. Radtke (2000). ESR dating stratigraphically well-constrained marine terraces along the Patagonian Atlantic coast (Argentina). *Quaternary International 68*, 261–273.

Schellmann, G. and U. Radtke (2003). Coastal terraces and Holocene sea-level changes along the Patagonian Atlantic coast. *Journal of Coastal Research*, 983–996.

Scussolini, P., J. Dullaart, S. Muis, A. Rovere, P. Bakker, D. Coumou, H. Renssen, P. J. Ward, and J. C. J. H. Aerts (2023). Modeled storm surge changes in a warmer world: the Last Interglacial. *Climate of the Past 19*(1), 141–157.

Senechal, N., G. Coco, K. R. Bryan, and R. A. Holman (2011). Wave runup during extreme storm conditions. *Journal of Geophysical Research: Oceans 116*(C7).

Shennan, I. (1986). Flandrian sea-level changes in the Fenland. II: Tendencies of sea-level movement, altitudinal changes, and local and regional factors. *Journal of Quaternary Science 1*(2), 155–179.

Shennan, I. (2015). Handbook of sea-level research: framing research questions. *Handbook of sea-level research*, 3–25.

Smith, C., T. Salles, and A. Vila-Concejo (2020). RADWave: Python code for ocean surface wave analysis by satellite radar altimeter. *Journal of Open Source Software 5*(47), 2083.

Stockdon, H. F., R. A. Holman, P. A. Howd, and A. H. Sallenger (2006). Empirical parameterization of setup, swash, and runup. *Coastal Engineering 53*(7), 573–588.

Styron, R. (2019). GEMScienceTools/gem-global-active-faults: First release of 2019.

Sulzbach, R., V. Klemann, G. Knorr, H. Dobslaw, H. Dümpelmann, G. Lohmann, and M. Thomas (2023). Evolution of Global Ocean Tide Levels Since the Last Glacial Maximum. *Paleoceanography and Paleoclimatology 38*(5), e2022PA004556.

Sunamura, T. (1992). *Geomorphology of rocky coasts*, Volume 3. Wiley.

Tamura, T. (2012). Beach ridges and prograded beach deposits as palaeoenvironment records. *Earth-Science Reviews 114*(3-4), 279–297.

Taylor, M. and G. W. Stone (1996). Beach-ridges: a review. *Journal of Coastal Research*, 612–621.

Tolman, H. L. et al. (2009). User manual and system documentation of WAVEWATCH III TM version 3.14. *Technical note, MMAB contribution 276*(220).

US Geological Survey, E. H. P. (2017). Advanced National Seismic System (ANSS) comprehensive catalog of earthquake events and products: Various.

Van de Plassche, O. (2013). *Sea-level Research: a Manual for the Collection and Evaluation of Data*. Springer.

Vos, K., M. D. Harley, K. D. Splinter, A. Walker, and I. L. Turner (2020). Beach Slopes From Satellite-Derived Shorelines. *Geophysical Research Letters 47*(14), e2020GL088365.

Vos, K., K. D. Splinter, M. D. Harley, J. A. Simmons, and I. L. Turner (2019). CoastSat: A Google Earth Engine-enabled Python toolkit to extract shorelines from publicly available satellite imagery. *Environmental Modelling & Software 122*, 104528.

Vousdoukas, M. I., D. Wziatek, and L. P. Almeida (2012). Coastal vulnerability assessment based on video wave run-up observations at a mesotidal, steep-sloped beach. *Ocean Dynamics 62*, 123–137.

Wilmes, S., V. K. Pedersen, M. Schindelegger, and J. A. M. Green (2023). Late Pleistocene Evolution of Tides and Tidal Dissipation. *Paleoceanography and Paleoclimatology 38*(11), e2023PA004727.

Yan, Q., R. Korty, T. Wei, and N. Jiang (2021). A Westward Shift in Tropical Cyclone Potential Intensity and Genesis Regions in the North Atlantic During the Last Interglacial. *Geophysical Research Letters 48*(12).

Zanchetta, G., I. Consoloni, I. Isola, M. Pappalardo, A. Ribolini, M. Aguirre, E. Fucks, I. Baneschi, M. Bini, L. Ragaini, et al. (2012). New insights on the Holocene marine transgression in the Bahía Camarones (Chubut, Argentina). *Italian Journal of Geosciences 131*(1), 19–31.

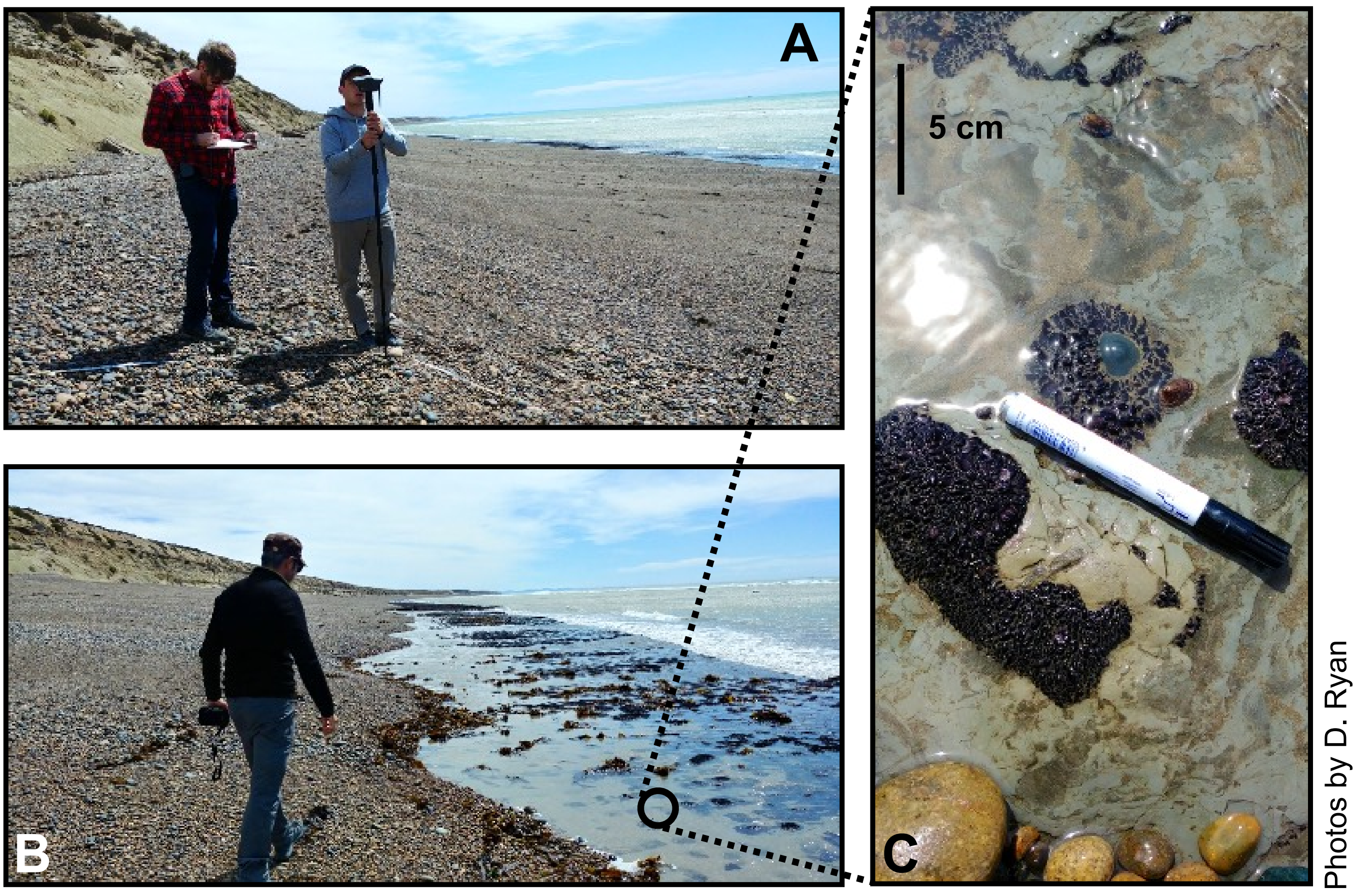

Supplementary Figure 1: Details of the modern beach at the benchmark site (Figure 2). A) view of the modern storm berm. B) lower part of the beach, with the exposed shore platform at low tide. C) detail of the shore platform, with encrusting organisms living on it.

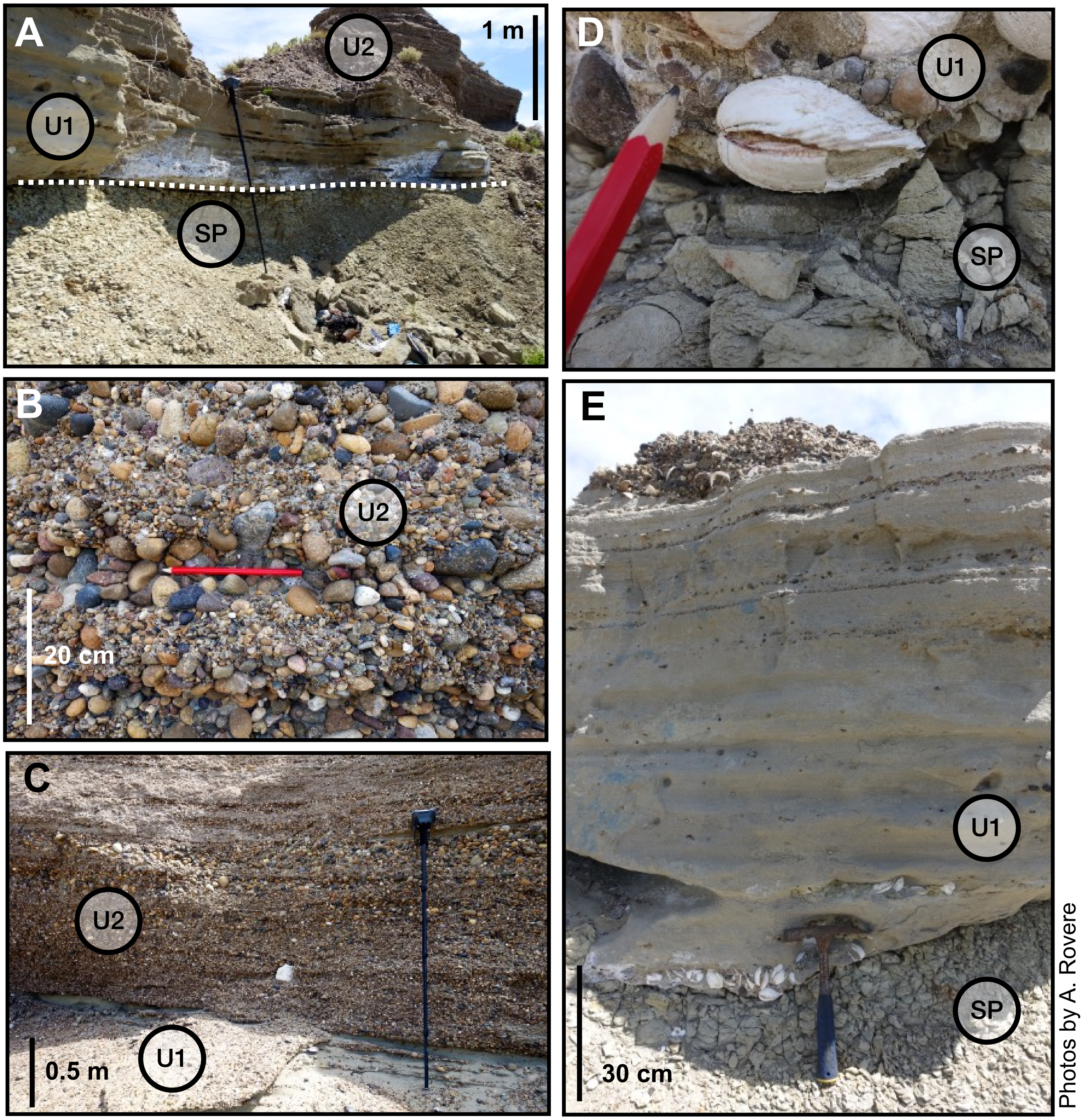

Supplementary Figure 2: Results of the runup calculations, divided by model employed, for waves perpendicular to the shore reaching the coast in tidal conditions above MSL.

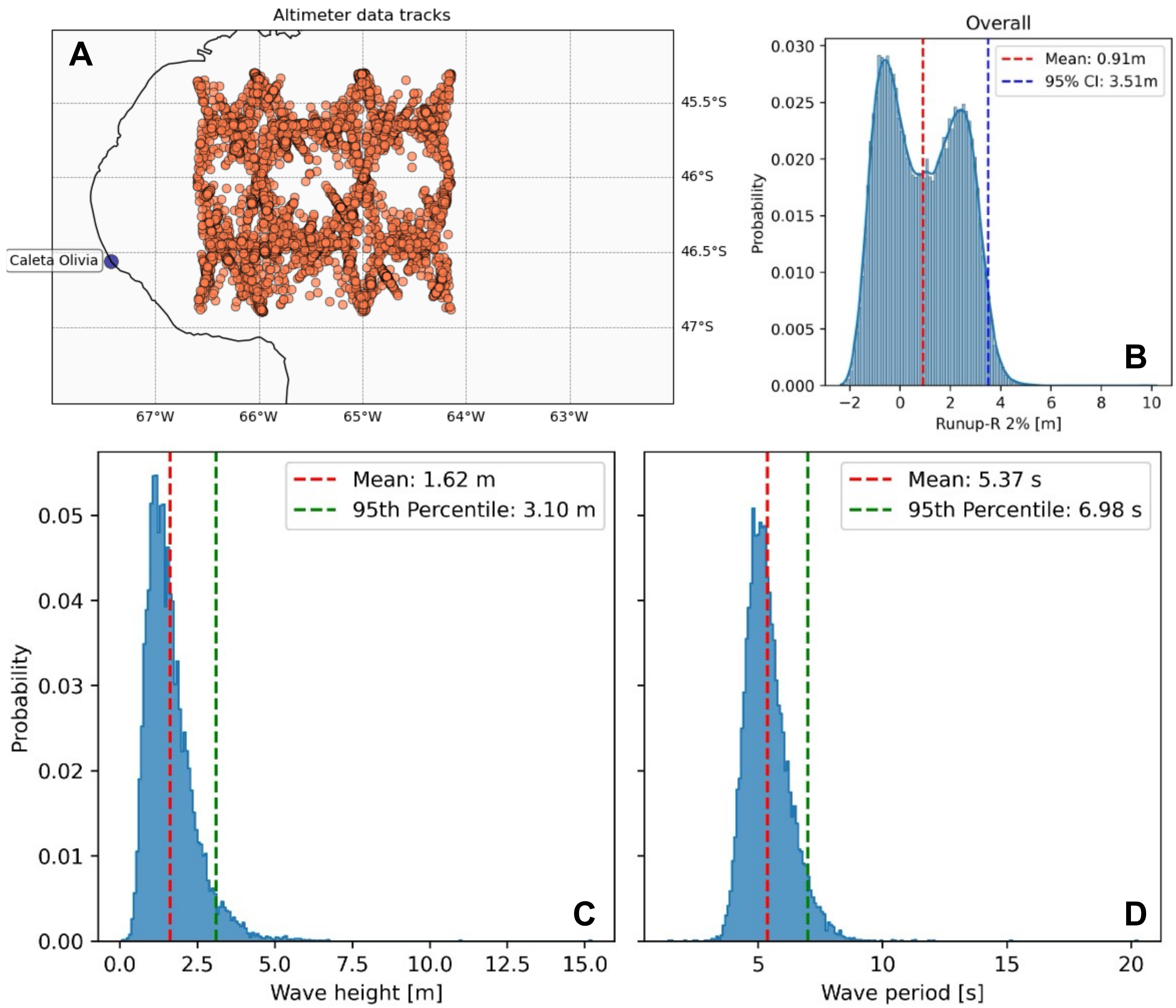

Supplementary Figure 3: A) satellite altimetry data tracks exported by the RADWave software. B) Wave runup calculated at Caleta Olivia with the approach of Rubio-Sandoval et al. (2024). C) and D) respectively wave height and period extracted from the satellite altimetry data.

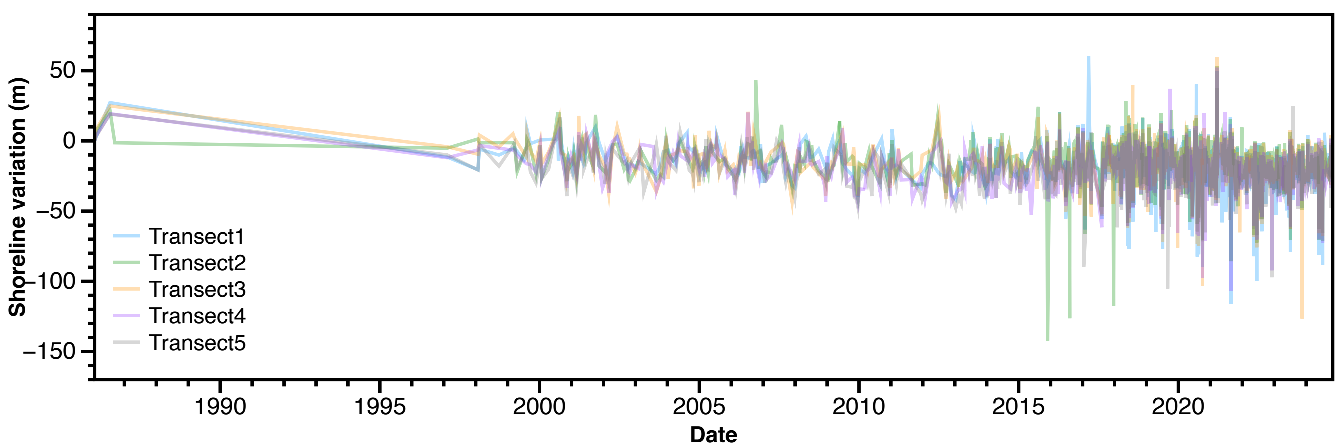

Supplementary Figure 4: Shoreline variations extracted with CoastSat (Vos et al., 2019) along the five transects using satellite imagery collected between 25 Jan 1986 and 30 Oct 2024.

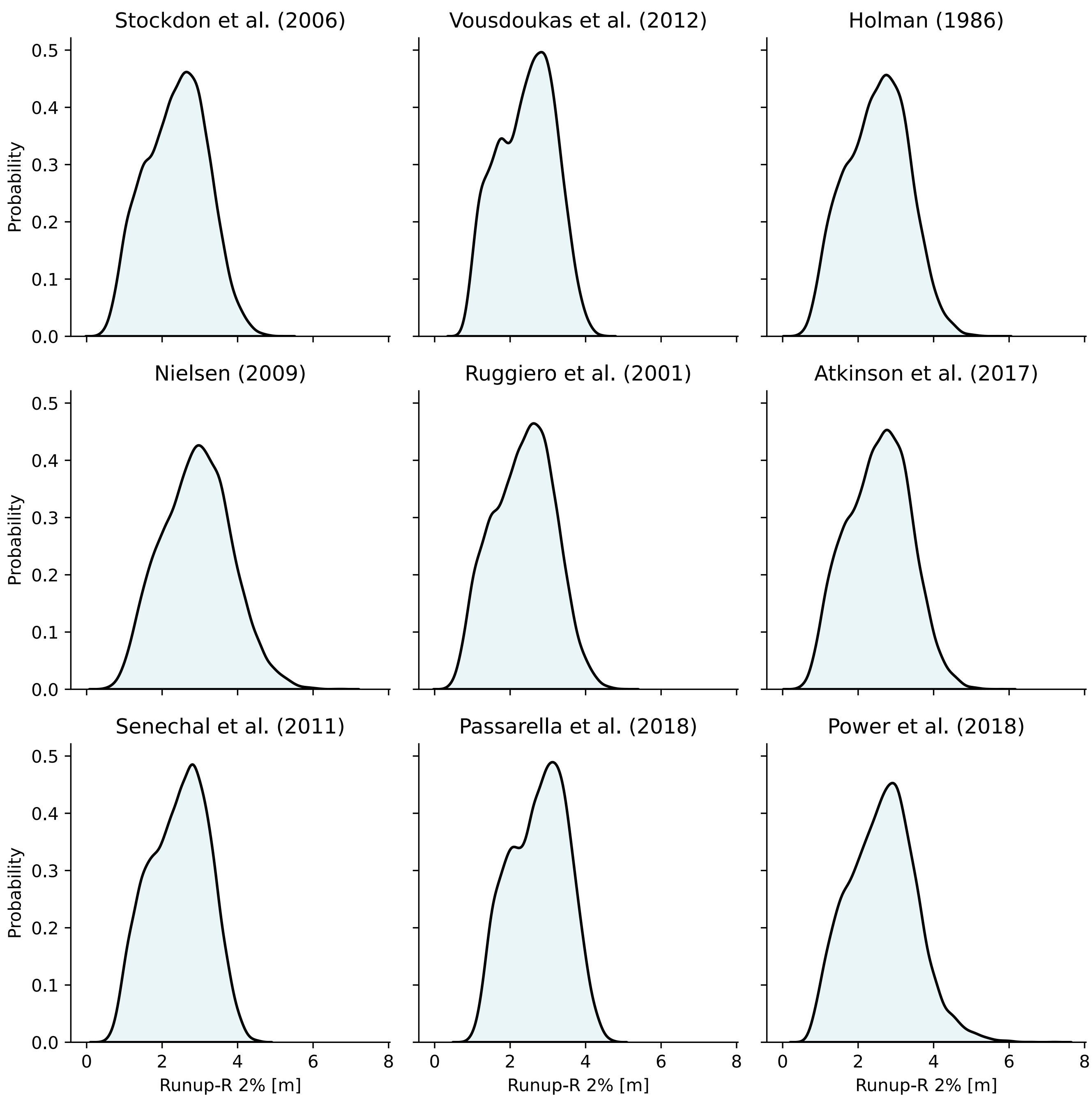

Supplementary Figure 5: Results of the different runup models used in this work. Only the runup values above MSL are shown here.

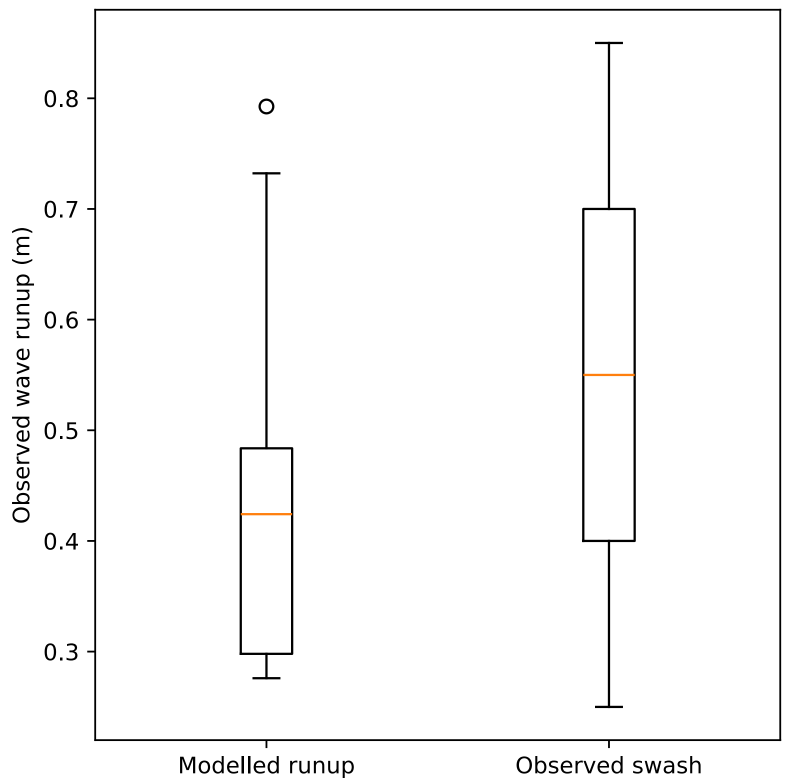

Supplementary Figure 6: Comparison between modelled and observed swash height at the time of survey (11 Feb 2019, 15.55 PM).

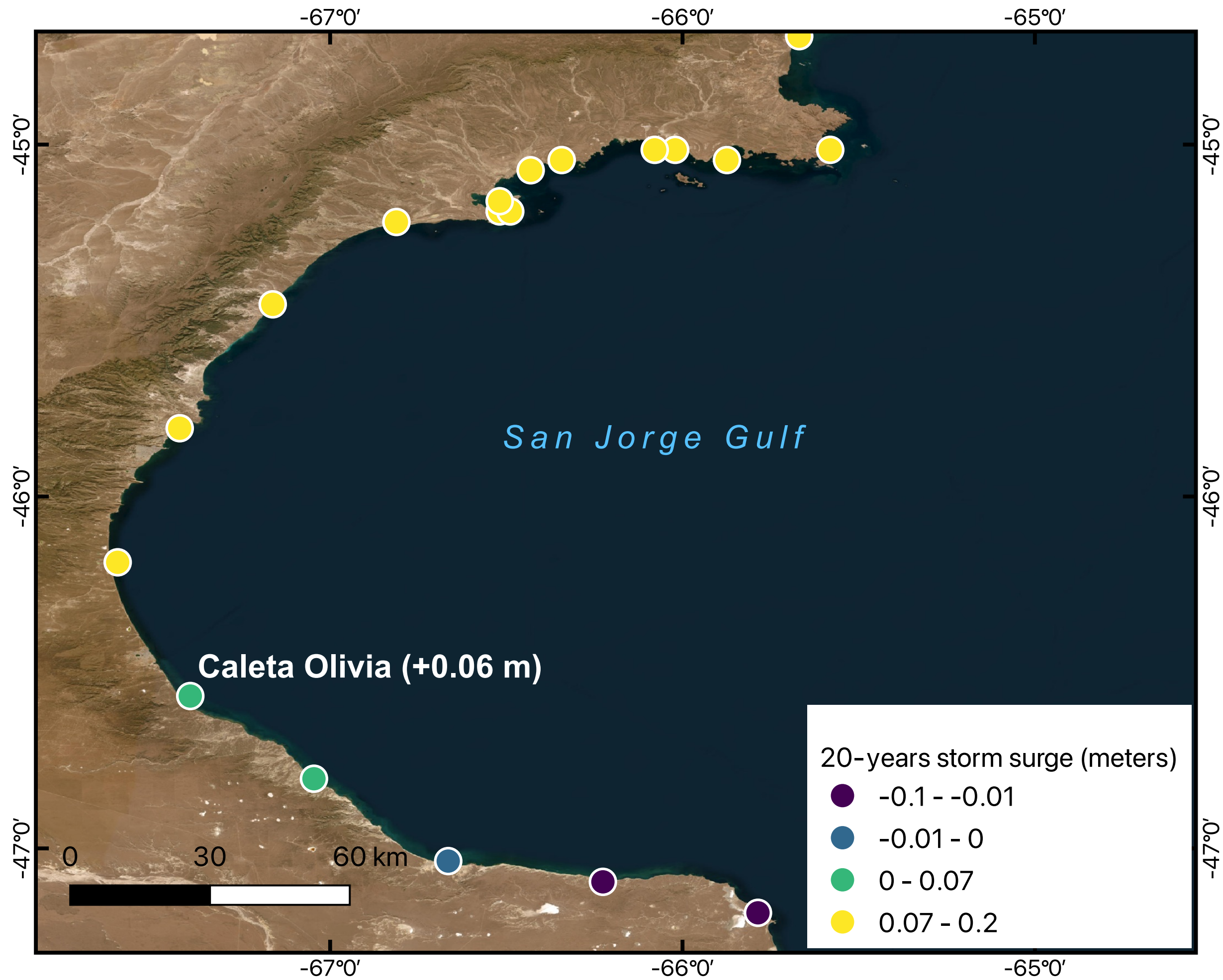

Supplementary Figure 7: Annual anomalies (Last Interglacial minus Present Interglacial) in sea level extremes at the 20-year return period in the San Jorge Gulf (Scussolini et al., 2023). Background imagery from ESRI ArcGIS Pro (World Imagery), source: Earthstar Geographics (TerraColor NextGen)

.